Hindawi Publishing Corporation
International Journal of Photoenergy
Volume 2013, Article ID 158496, 7 pages
http://dx.doi.org/10.1155/2013/158496

Research Article

A Cost-Effective Solid-State Approach to Synthesize g-C_3N_4 Coated TiO_2 Nanocomposites with Enhanced Visible Light Photocatalytic Activity

Min Fu, Junmin Pi, Fan Dong, Qiuyan Duan, and Huan Guo

Chongqing Laboratory of Catalysis and Functional Organic Molecules, College of Environmental and Biological Engineering, Chongqing Technology and Business University, Chongqing 400067, China

Correspondence should be addressed to Min Fu; fumin1022@126.com and Fan Dong; dfctbu@126.com

Received 22 June 2013; Accepted 2 September 2013

Academic Editor: Guisheng Li

Novel graphitic carbon nitride (g-C_3N_4) coated TiO_2 nanocomposites were prepared by a facile and cost-effective solid-state method by thermal treatment of the mixture of urea and commercial TiO_2. Because the C_3N_4 was dispersed and coated on the TiO_2 nanoparticles, the as-prepared g-C_3N_4/TiO_2 nanocomposites showed enhanced absorption and photocatalytic properties in visible light region. The as-prepared g-C_3N_4 coated TiO_2 nanocomposites under 450°C exhibited efficient visible light photocatalytic activity for degradation of aqueous MB due to the increased visible light absorption and enhanced MB adsorption. The g-C_3N_4 coated TiO_2 nanocomposites would have wide applications in both environmental remediation and solar energy conversion.

1. Introduction

Visible light photocatalysis has attracted the worldwide attention due to its potential application in environmental remediation and solar energy conversion [1–7]. The photocatalyst TiO_2, however, can only utilize the ultraviolet light (about 5% of natural solar light) because of its wide band gap (ca. 3.2 eV for anatase TiO_2). During the past 40 years, many efforts have been devoted to enhance the visible light photocatalytic activity of TiO_2, including metal doping [8–10], nonmetal doping [11–14], surface modification [15], and heterojunction construction [16–19].

In recent years, polymeric g-C_3N_4 materials have attracted much attention because of their similarity to graphene. Zhang et al. reported that the polymeric g-C_3N_4 semiconductors exhibit high photocatalytic performance for water splitting under visible light irradiation [20]. Dong and coworkes reported that polymeric g-C_3N_4 layered materials as novel efficient visible light photocatalyst, which can be synthesized facilely by directly heating urea or thiourea [21, 22].

Very recently, Zhou et al. reported a g-C_3N_4/TiO_2 nanotube array heterojunction with excellent visible light photocatalytic activity [17]. Zhao et al. reported g-C_3N_4/TiO_2 hybrids with wide absorption wavelength and effective photogenerated charge separation [18]. However, the precursors for g-C_3N_4 (dicyandiamide and melamine) are poisonous and detrimental to the environment. The preparation processes were relatively tedious, which may prevent large-scale application [17, 18].

In the present work, g-C_3N_4/TiO_2 nanocomposites were prepared by a facile and cost-effective solid-state method using urea and commercial TiO_2 as precursors. It was interesting to find that g-C_3N_4 was *in situ* coated on the surface of TiO_2. The precursors (urea and commercial TiO_2) are low cost and easily available. The as-prepared g-C_3N_4 coated TiO_2 nanocomposites exhibited enhanced photocatalytic activity under visible light irradiation.

2. Experimental

2.1. Synthesis. The g-C_3N_4 coated TiO_2 nanocomposites were prepared by a facile and cost-effective solid-state method. In a typical synthesis, 2 g TiO_2 and 6 g urea were immersed in 10 mL H_2O and dried at 60°C to completely remove the water.

The mixtures were put into an alumina crucible with a cover, and then heated to a certain temperature in the range of 400 and 600°C in a muffle furnace for 1 h at a heating rate of 15°C min^{-1}. The final samples were collected for use without further treatment.

2.2. Characterization. The crystal phases of the sample were analyzed by X-ray diffraction with Cu Kα radiation (XRD: model D/max RA, Rigaku Co., Japan). The morphology and structure of the samples were examined by transmission electron microscopy (TEM: JEM-2010, Japan). The UV-vis diffuse reflection spectra were obtained for the dry-pressed disk samples using a Scan UV-Vis spectrophotometer (UV-Vis DRS: UV-2450, Shimadzu, Japan) equipped with an integrating sphere assembly, using $BaSO_4$ as reflectance sample. The spectra were recorded at room temperature in air range from 250 to 800 nm. X-ray photoelectron spectroscopy with Al Kα X-rays ($h\nu$ = 1486.6 eV) radiation operated at 150 W (XPS: Thermo ESCALAB 250, USA) was used to investigate the surface properties. The shift of the binding energy due to relative surface charging was corrected using the C1s level at 284.8 eV as an internal standard. FT-IR spectra were recorded on a Nicolet Nexus spectrometer on samples embedded in KBr pellets. The nitrogen adsorption-desorption isotherms were determined by the BET method (BET-BJH: ASAP 2020, USA), from which the surface area, pore volume, and average pore diameter were calculated by using the BJH method. All the samples were degassed at 200°C prior to measurements.

2.3. Evaluation of Photocatalytic Activity. Photocatalytic activity of g-C_3N_4/TiO_2 for MB photodegradation was evaluated in a quartz glass reactor. 0.05 g of N-TiO_2 was dispersed in MB aqueous solution (50 mL, 5 mg/L). The light irradiation system contains a 500 W Xe lamp with a jacket filled with flowing and thermostated aqueous $NaNO_2$ solution (1 M) between the lamp and the reaction chamber as a filter to block UV light ($\lambda < 400$ nm) and eliminate the temperature effect. The suspension was first allowed to reach adsorption-desorption equilibrium with continuous stirring for 60 min in the dark prior to irradiation. The degradation rate of MB was evaluated using the UV-Vis absorption spectra to measure the peak value of a maximum absorption of MB solution. During the irradiation, 5 mL of suspension was continually taken from the reaction cell at given time intervals for subsequent dye concentration analysis after centrifugation. The MB solution shows a similar pH value at 6.8, which does not affect the light absorption of MB. The maximum absorption of MB is at wavelength of 665 nm. The degradation rate η (%) can be calculated as

$$\eta\,(\%) = \frac{(C_0 - C)}{C_0} \times 100\%, \quad (1)$$

where C_0 is the initial concentration of MB considering MB adsorption on the catalyst and C is the revised concentration after irradiation.

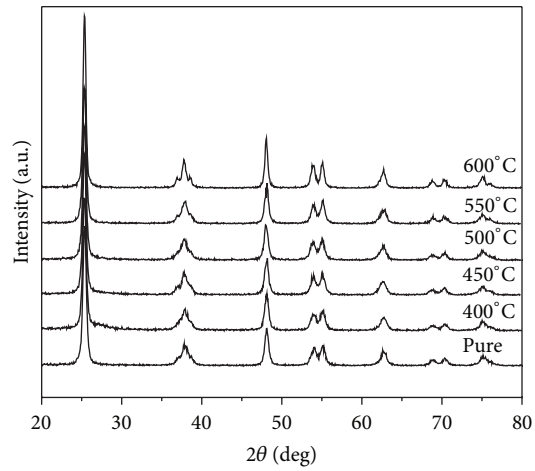

Figure 1: XRD patterns of the C_3N_4/TiO_2 nanocomposites obtained under different temperatures.

3. Results and Discussion

Figure 1 shows the XRD patterns of the as-prepared g-C_3N_4 coated TiO_2 nanocomposites at different temperatures. The peaks of all the samples can be indexed to the anatase phase of TiO_2 (JCPDS file No. 21-1272). It can be seen that the peak intensity increases gradually under higher treatment temperature, which indicates that the crystal sizes of TiO_2 nanocomposites increase under higher treatment temperature. No typical peaks of g-C_3N_4 can be found for all the samples due to the fact that g-C_3N_4 with layered structures on the surface of TiO_2 is ultrathin (Figure 2) and the crystallinity is low [22].

The morphology of pure TiO_2 and g-C_3N_4/TiO_2 nanocomposites were observed by TEM. As shown in Figure 2, both samples contain a number of monodispersed nanoparticles of TiO_2 with a size of about 11 nm. The intra-aggregation of particles could form the mesoporous structure [23]. It can be seen from Figure 2(b) that the ultrathin g-C_3N_4 with layered structures are dispersed and coated on the surface of TiO_2 particles, which is consistent with absence of the peaks of g-C_3N_4 in XRD (Figure 1).

The FT-IR spectra of pure TiO_2 and g-C_3N_4 coated TiO_2 nanocomposites are shown in Figure 3(a). The absorption band around 400–800 cm^{-1} is attributed to Ti–O bonds [23]. Several bands in the range of 1100–1650 cm^{-1} correspond to the typical stretching vibration of CN heterocycles in g-C_3N_4. The characteristic vibration mode of triazine units can also be found at 801 cm^{-1} [22]. The peak at 1630 cm^{-1} is associated with the stretching vibration of water molecules for both samples, including molecular water and hydroxyl groups [23]. The FT-IR spectra further confirm the existence of g-C_3N_4 on the surface of TiO_2.

The TG and DSC thermograms (Figure 3(b)) show that there are several phase transformations during heating. An endothermal peak at 135°C is the melting point of urea. The peak at 242°C indicates the reaction of urea into melamine. The weight loss during the two stages decreases rapidly by 36.1%. The sharp peak at 367°C implies that the thermal

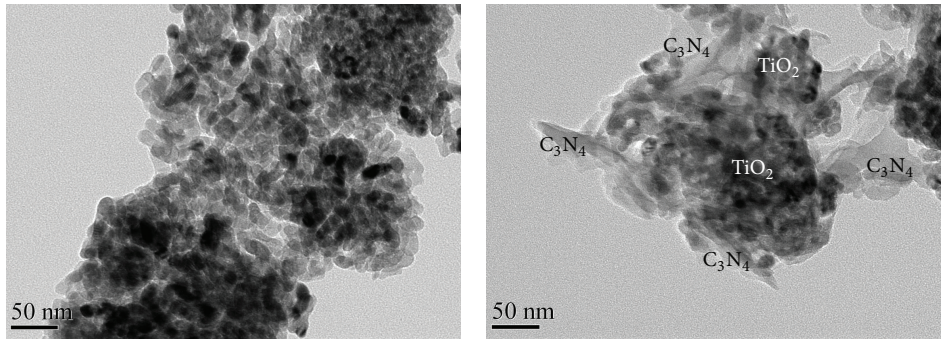

(a) (b)

Figure 2: TEM images of pure TiO_2 (a) and g-C_3N_4/TiO_2 nanocomposites sample obtained under 450°C (b).

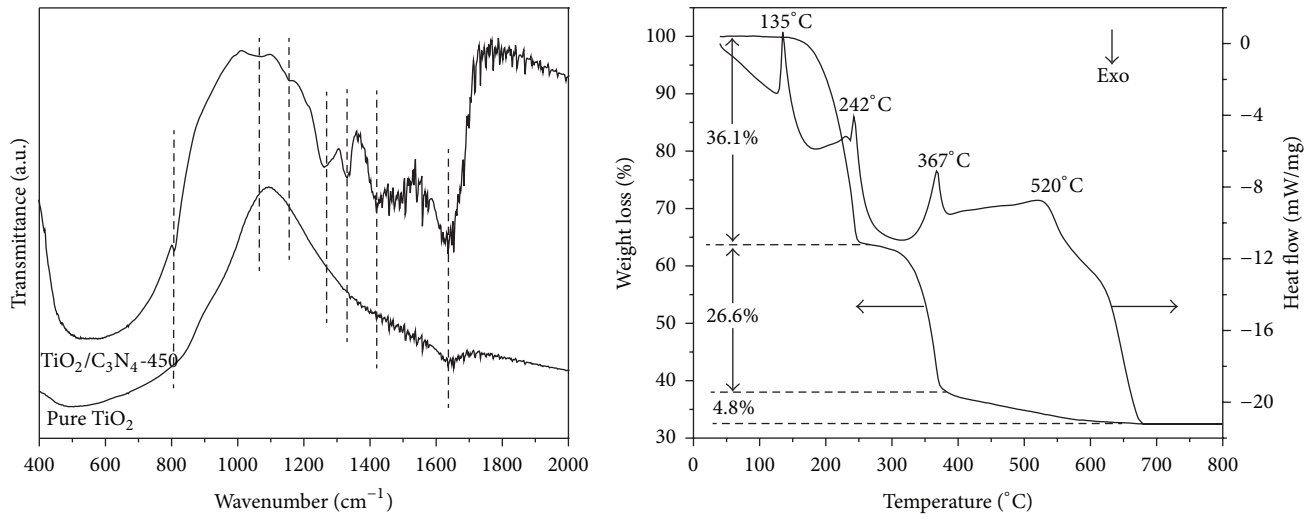

(a) (b)

Figure 3: FTIR spectra of pure TiO_2 and g-C_3N_4/TiO_2 nanocomposites (a) and TG-DSC for heating the mixture of TiO_2 and urea (b).

condensation of melamine into g-C_3N_4 occurred in this temperature range. The weight loss in this stage is about 26.6%. The further weight loss of 4.8% with endothermal peak at 520°C can be attributed to the decomposition of g-C_3N_4. The TG-DSC result implies that g-C_3N_4 can be *in situ* formed on the surface of TiO_2, which is consistent with Figure 2(b).

The C1s spectra in Figure 4(a) show that two main carbon species with binding energies of 284.9 and 288.1 eV, corresponding to C–C and C–N–C, respectively. Three binding energies in N1s region (Figure 4(b)) can be observed, which can be indexed to C–N–C (398.8 eV), N–$(C)_3$ (400.1 eV), and N–H groups (401.2 eV), respectively. The binding energy at 529.7 and 533.0 eV can be ascribed to Ti–O, surface hydroxyl groups, and adsorbed molecular water (Figures 4(c) and 4(d)) [22]. The XPS results are consistent with the FT-IR spectra. XPS results also indicate that no peak for Ti–C or Ti–N bond can be observed, which implies that there is no chemical bond connection between g-C_3N_4 and TiO_2.

The nitrogen adsorption-desorption isotherms of pure TiO_2 and g-C_3N_4/TiO_2 nanocomposites obtained under 450°C are shown in Figure 5(a). The two samples show a type IV adsorption isotherm with a H_2 hysteresis loop in the range (P/P_0) of 0.6–1.0, which indicates the presence of mesopores. The surface areas and pore volume of pure TiO_2 are 78 m^2/g and 0.281 cm^3/g, higher than those of g-C_3N_4/TiO_2 nanocomposites (48 m^2/g and 0.216 cm^3/g). The pore size distribution curve (Figure 5(b)) indicates that the large mesopores of pure TiO_2 and g-C_3N_4/TiO_2 nanocomposites are about 37 and 48 nm, respectively. The presence of large mesopores can be ascribed to the aggregation of TiO_2 particles. It can be observed that the g-C_3N_4/TiO_2 nanocomposites have small mesopores of around 13.6 nm (inset in Figure 5(b)), which originates from the presence of layered g-C_3N_4 on the TiO_2 surface. The small mesopore is advantageous for enhancing the adsorption for reactant.

Figure 6 shows the UV-Vis DRS spectra of pure TiO_2 and the as-prepared g-C_3N_4/TiO_2 nanocomposites. It is clear that the visible light absorption of g-C_3N_4/TiO_2 nanocomposites is enhanced with increased treatment temperatures until 450°C. Then the visible light absorption decreases when the temperature is higher than 450°C. This fact implies

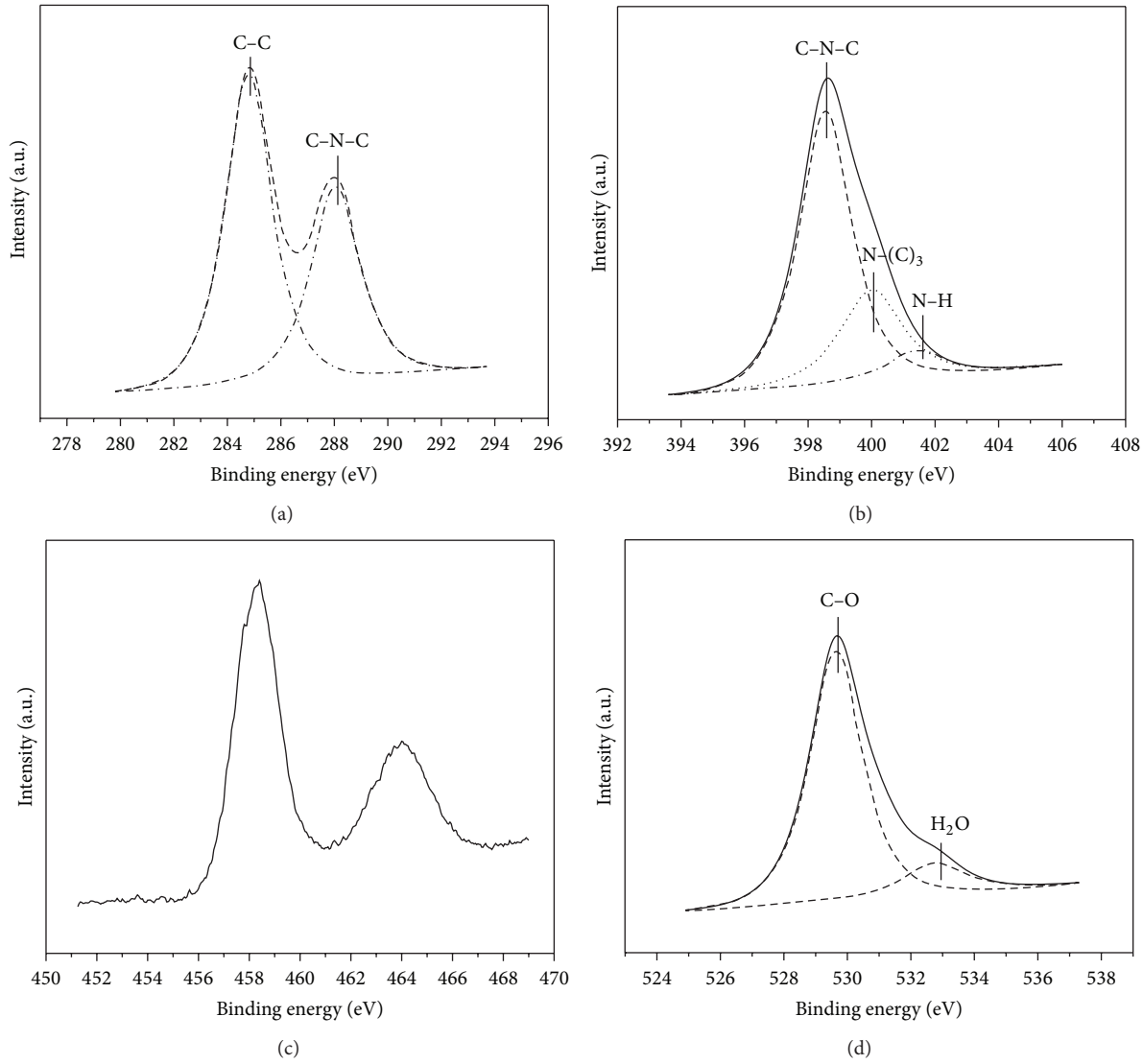

Figure 4: XPS spectra of the as-prepared C_3N_4 coated TiO_2 nanocomposite under 450°C.

that the as-prepared g-C_3N_4 coated TiO_2 nanocomposites under 450°C may exhibit excellent visible light photocatalytic activity. However, the decrease of visible light absorption intensity of coated TiO_2 nanocomposites under higher treatment temperature can be attributed to the decomposition of g-C_3N_4.

Figure 7 shows the adsorption and photocatalytic activity of pure TiO_2 and g-C_3N_4/TiO_2 nanocomposites for removal of MB. It can be seen that the g-C_3N_4/TiO_2 nanocomposites obtained under 450°C exhibit the highest adsorption capacity, which may be ascribed to presence of layered g-C_3N_4 and small mesopores of the nanocomposites sample. The photocatalytic activities of g-C_3N_4/TiO_2 nanocomposites first increase and then decrease with the increased treatment temperature. Pure TiO_2 shows low visible light activity due to its large band gap. The observed slight visible light activity for the pure TiO_2 sample can be ascribed to the photosensitization effect of the MB as MB can absorb visible light [18]. During the visible light irradiation, the part of MB was self-decomposed due to the photosensitization. When TiO_2 was coated by g-C_3N_4, all the nanocomposite samples show decent visible light activity. Under visible light irradiation, g-C_3N_4 with a band gap of 2.7 eV could be excited and the photogenerated electrons could transfer from the conduction band (CB) of g-C_3N_4 to the CB of TiO_2 [17, 18, 24]. The holes in the valence band (VB) of g-C_3N_4 and electrons on the CB of TiO_2 could initiate the following degradation reactions. The as-prepared g-C_3N_4/TiO_2 nanocomposites under 450°C exhibit the highest photocatalytic activity under visible light irradiation. Considering the fact that the surface area of g-C_3N_4/TiO_2 nanocomposites (48 m^2/g) is lower than that of pure TiO_2 (78 m^2/g), the surface area of g-C_3N_4/TiO_2 is not a positive factor. The enhanced visible light activity of g-C_3N_4/TiO_2 should be ascribed to the enhanced visible light adsorption because of the presence of g-C_3N_4 (Figures 2(b) and 6) and the improved MB adsorption

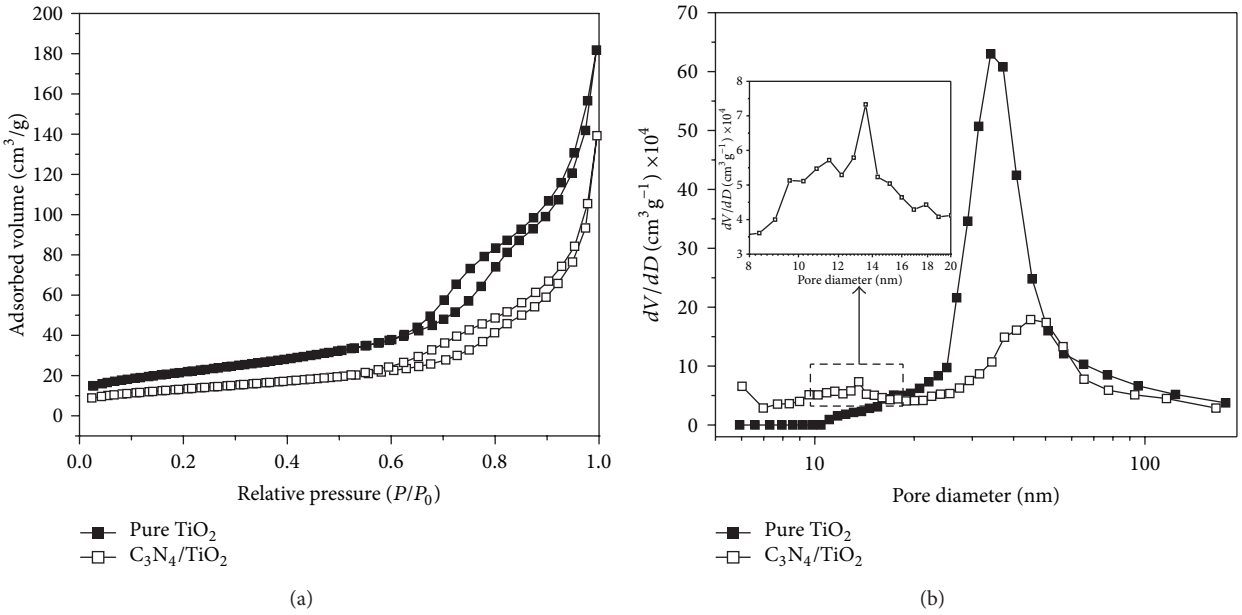

Figure 5: BET-BJH of the pure TiO_2 and C_3N_4 coated TiO_2 nanocomposite obtained under 450°C.

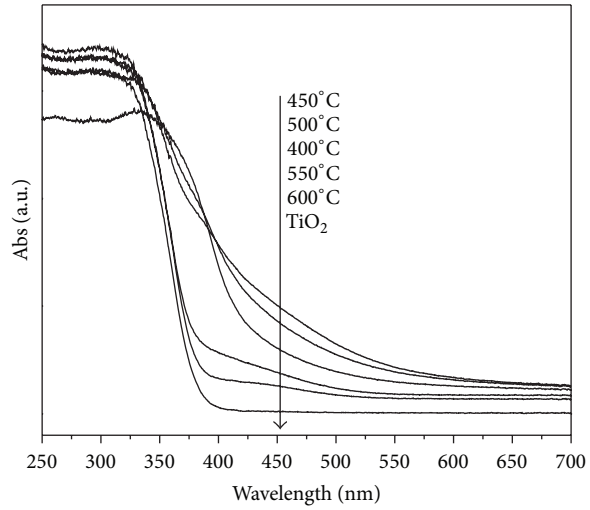

Figure 6: UV-Vis DRS of the pure TiO_2 and g-C_3N_4/TiO_2 samples obtained under different temperatures.

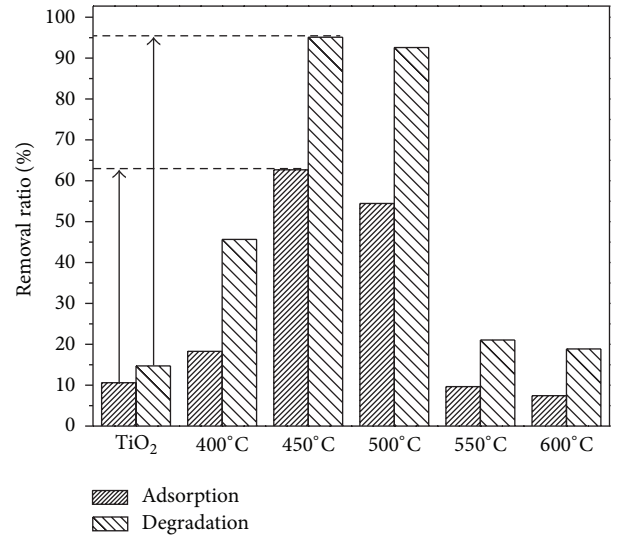

Figure 7: Adsorption and photocatalytic activity of the pure TiO_2 and g-C_3N_4/TiO_2 samples obtained under different temperatures for removal of MB.

because of the small mesopores of the nanocomposites sample (Figure 5(b)). As the precursors (urea and commercial TiO_2) are cheap and preparation method is very simple, the as-prepared g-C_3N_4 coated TiO_2 nanocomposites are ready for large-scale applications in environmental pollution control and solar energy conversion [25].

4. Conclusion

The g-C_3N_4/TiO_2 nanocomposites were synthesized by a cost-effective solid-state approach by thermal treatment of the mixture of urea and commercial TiO_2. It was found that the surface of TiO_2 particles was coated by the *in situ* formed thin layered g-C_3N_4 from urea. The adsorption capacity and visible light photocatalytic activity were significantly enhanced. Under the optimized treatment temperature of 450°C, the g-C_3N_4/TiO_2 nanocomposites exhibited highest adsorption capacity and visible light photocatalytic activity toward removal of MB. The enhanced adsorption capacity can be ascribed to the presence of g-C_3N_4 and small mesopores. The enhanced visible photocatalytic activity originated from the increased visible light adsorption and small mesopores of the nanocomposites sample. The novel

g-C_3N_4 coated TiO_2 nanocomposites prepared by the cost-effective solid-state approach would find wide application in environmental remediation.

Conflict of Interests

The authors declare no conflict of interests.

Acknowledgments

This research is financially supported by the Key Project from CQ CSTC (cstc2013yykfB50008), the Science and Technology Project from Chongqing Education Commission (KJZH11214, KJ120713, KJTD201314, KJTD201020, KJ130725, and KJ090727), the Key Discipline Development Project of CTBU (1252001), the National Natural Science Foundation of China (51108487), and the Natural Science Foundation Project of CQ CSTC (cstc2012jjA20014, CSTC2010BB0260).

References

[1] J. Zhang, J. Sun, K. Maeda et al., "Sulfur-mediated synthesis of carbon nitride: band-gap engineering and improved functions for photocatalysis," *Energy and Environmental Science*, vol. 4, no. 3, pp. 675–678, 2011.

[2] Y. J. Cui, Z. X. Ding, X. Z. Fu, and X. C. Wang, "Construction of conjugated carbon nitride nanoarchitectures in solution at low temperatures for photoredox catalysis," *Angewandte Chemie—International Edition*, vol. 51, no. 47, pp. 11814–11818, 2012.

[3] Z. Z. Lin and X. C. Wang, "Nanostructure engineering and doping of conjugated carbon nitride semiconductors for hydrogen photosynthesis," *Angewandte Chemie—International Edition*, vol. 52, no. 6, pp. 1735–1738, 2013.

[4] Q. Y. Chen and D. Ma, "Preparation of nanostructured Cu_2SnS_3 photocatalysts by solvothermal method," *International Journal of Photoenergy*, vol. 2013, Article ID 593420, 5 pages, 2013.

[5] N. Todorova, T. Giannakopoulou, G. Romanos, T. Vaimakis, J. Yu, and C. Trapalis, "Preparation of fluorine-doped TiO_2 photocatalysts with controlled crystalline structure," *International Journal of Photoenergy*, vol. 2008, Article ID 534038, 9 pages, 2008.

[6] Q. Xiang, J. Yu, and M. Jaroniec, "Graphene-based semiconductor photocatalysts," *Chemical Society Reviews*, vol. 41, no. 2, pp. 782–796, 2012.

[7] X. Li, P. Zhang, L. Jin, T. Shao, Z. Li, and J. Cao, "Efficient photocatalytic decomposition of perfluorooctanoic acid by indium oxide and its mechanism," *Environmental Science and Technology*, vol. 46, no. 10, pp. 5528–5534, 2012.

[8] Z. Wu, Z. Sheng, H. Wang, and Y. Liu, "Relationship between Pd oxidation states on TiO_2 and the photocatalytic oxidation behaviors of nitric oxide," *Chemosphere*, vol. 77, no. 2, pp. 264–268, 2009.

[9] M. Fu, Y. Li, S. Wu, P. Lu, J. Liu, and F. Dong, "Sol-gel preparation and enhanced photocatalytic performance of Cu-doped ZnO nanoparticles," *Applied Surface Science*, vol. 258, no. 4, pp. 1587–1591, 2011.

[10] X. W. Cheng, X. J. Yu, B. Y. Li, L. Yan, Z. P. Xing, and J. J. Li, "Enhanced visible light activity and mechanism of TiO_2 codoped with molybdenum and nitrogen," *Materials Science and Engineering B*, vol. 178, no. 7, pp. 425–430, 2013.

[11] Z. H. Ai, Z. T. Gao, K. Su, W. K. Ho, and L. Z. Zhang, "Aerosol flow synthesis of N, Si-codoped TiO_2 hollow microspheres with enhanced visible-light driven photocatalytic performance," *Catalysis Communications*, vol. 29, no. 5, pp. 189–193, 2012.

[12] F. Dong, W. Zhao, and Z. Wu, "Characterization and photocatalytic activities of C, N and S co-doped TiO_2 with 1D nanostructure prepared by the nano-confinement effect," *Nanotechnology*, vol. 19, no. 36, Article ID 365607, 2008.

[13] P. Periyat, D. E. McCormack, S. J. Hinder, and S. C. Pillai, "One-pot synthesis of anionic (nitrogen) and cationic (sulfur) codoped high-temperature stable, visible light active, anatase photocatalysts," *Journal of Physical Chemistry C*, vol. 113, no. 8, pp. 3246–3253, 2009.

[14] H. Wang, Z. B. Wu, and Y. Liu, "A simple two-step template approach for preparing carbon-doped mesoporous TiO_2 hollow microspheres," *Journal of Physical Chemistry C*, vol. 113, no. 30, pp. 13317–13324, 2009.

[15] F. Chen, W. Zou, W. Qu, and J. Zhang, "Photocatalytic performance of a visible light TiO_2 photocatalyst prepared by a surface chemical modification process," *Catalysis Communications*, vol. 10, no. 11, pp. 1510–1513, 2009.

[16] F. Dong, Y. J. Sun, and M. Fu, "Enhanced visible light photocatalytic activity of V_2O_5 cluster modified N-doped TiO_2 for degradation of toluene in air," *International Journal of Photoenergy*, vol. 2012, Article ID 569716, 10 pages, 2012.

[17] X. S. Zhou, B. Jin, L. D. Li et al., "A carbon nitride/TiO_2 nanotube array heterojunction visible-light photocatalyst: synthesis, characterization, and photoelectrochemical properties," *Journal of Materials Chemistry*, vol. 22, no. 34, pp. 17900–179055, 2012.

[18] S. S. Zhao, S. Chen, H. T. Yu, and X. Quan, "g-C_3N_4/TiO_2 hybrid photocatalyst with wide absorption wavelength range and effective photogenerated charge separation," *Separation and Purification Technology*, vol. 99, no. 8, pp. 50–54, 2012.

[19] J. G. Yu, S. H. Wang, B. Cheng, Z. Lin, and F. Huang, "Noble metal-free $Ni(OH)_2$-g-C_3N_4 composite photocatalyst with enhanced visible-light photocatalytic H_2-production activity," *Catalysis Science Technology*, vol. 3, no. 7, pp. 1782–1789, 2013.

[20] J. S. Zhang, M. W. Zhang, R. Q. Sun, and X. C. Wang, "A facile band alignment of polymeric carbon nitride semiconductors to construct isotype heterojunctions," *Angewandte Chemie—International Edition*, vol. 51, no. 40, pp. 10145–10149, 2012.

[21] F. Dong, L. Wu, Y. Sun, M. Fu, Z. Wu, and S. C. Lee, "Efficient synthesis of polymeric g-C_3N_4 layered materials as novel efficient visible light driven photocatalysts," *Journal of Materials Chemistry*, vol. 21, no. 39, pp. 15171–15174, 2011.

[22] F. Dong, Y. J. Sun, L. W. Wu, M. Fu, and Z. B. Wu, "Facile transformation of low cost thiourea into nitrogen-rich graphitic carbon nitride nanocatalyst with high visible light photocatalytic performance," *Catalysis Science and Technology*, vol. 2, no. 7, pp. 1332–1335, 2012.

[23] F. Dong, S. Guo, H. Wang, X. Li, and Z. Wu, "Enhancement of the visible light photocatalytic activity of C-doped TiO_2 nanomaterials prepared by a green synthetic approach," *Journal of Physical Chemistry C*, vol. 115, no. 27, pp. 13285–13292, 2011.

[24] S. K. Choi, S. Kim, S. K. Lim, and H. Park, "Photocatalytic comparison of TiO_2 nanoparticles and electrospun TiO_2 nanofibers: effects of mesoporosity and interparticle charge transfer," *Journal of Physical Chemistry C*, vol. 114, no. 39, pp. 16475–16480, 2010.

[25] W. D. Zhang, Q. Zhang, F. Dong, and Z. W. Zhao, "The multiple effects of precursors on the properties of polymeric carbon nitride," *International Journal of Photoenergy*, vol. 2013, Article ID 685038, 9 pages, 2013.